Carrier-envelope phase effects on high-harmonic generation driven by mid-infrared laser field*

Diao Han-Hu(刁寒虎), Zheng Ying-Hui(郑颖辉)†, Zhong Yue(钟 悦), Zeng Zhi-Nan(曾志男)‡, Ge Xiao-Chun(葛晓春), Li Chuang(李 闯), Li Ru-Xin(李儒新), and Xu Zhi-Zhan(徐至展)

Shanghai Institute of Optics and Fine Mechanics, Chinese Academy of Sciences, Shanghai 201800, *China*

(Received 5 April 2014; revised manuscript received 29 April 2014; published online 10 August 2014)

The influence of the carrier-envelope phase on high-harmonic generation is investigated, both experimentally and theoretically, for three different interaction gas media, driven by mid-infrared, few-cycle and CEP-stabilized laser pulses. Different patterns of harmonic spectra with varying CEP for the three interaction gas media are observed. Furthermore, in comparing our experiment results to the previous works driven by near-infrared laser pulses, different phenomena are found. Through numerical simulation, we find that for the two different kinds of driving fields, i.e. mid-infrared and near-infrared laser pulses, different kinds of electron trajectories contribute to the generation of high harmonics.

Keywords: high-harmonic generation, carrier-envelope phase, mid-infrared

PACS: 42.65.Ky, 32.80.Rm **DOI:** 10.1088/1674-1056/23/10/104210

1. Introduction

High-harmonic generation (HHG) was an outstanding discovery in the 20th century, for it not only provides a significant way to generate coherent XUV or X-ray light,[1,2] but also extends the time scale of microcosmic dynamics research to the never-before-accessed attosecond (1 as = 10^{-18} s) level.[3] Mainly two models are used to describe the mechanism of HHG. The first is the three-step model proposed by P. B. Corkum.[4–6] The three steps are: 1) a free electron is created through tunneling ionization; 2) the freed electron is accelerated by an electric field of a laser in its emitted continuum; 3) the electron recombines with its parent ion and liberates its electron energy in the form of harmonic photons. The second model is based on the principle of Feynman's path integral[7] and was derived by Lewenstein *et al.*[8] It represents the electron dynamics in the HHG process as the superposition of electron orbits (or electron trajectories) and the trajectories selected by saddle-point approximation.[9,10] After decades of development, to achieve the extreme process of HHG, researchers began to use few-cycle light pulses as the driving field.[11] Unlike the many-cycle regime, in which all processes are insensitive to the carrier-envelope phase (CEP), in the few-cycle situation the CEP is a key parameter for the driving field. The exact positions of the nodes and peaks of the electric field during the pulse determine the ionization and re-collision of the electron.[12] Many groups have made great efforts in researching CEP's effects on HHG,[13,14] i.e., cutoff energy,[15,16] half-cycle cutoff (HCO),[17] and HHG conversion efficiency.[18] However, most of the research on the CEP effects is based on driving lasers in the near-infrared (near-IR) spectral band (mostly 760 nm∼800 nm). Considering Corkum's three-step model, the cutoff energy can be estimated by: $\varepsilon = I_p + 3.17U_p$,[19] where I_p is the ionization energy of the interaction medium and $U_p = E_L^2/4\omega^2$ is the ponderomotive energy that is due to the laser field. Hence, to achieve even larger cutoff energy, a driving laser of longer wavelength was selected for our work. And recently, many groups have chosen mid-infrared (mid-IR) pulse laser as the driving source for HHG process.[20–22] Compared with the near-IR driver, in a mid-IR field, the freed electron spends more time in the continuum; hence, CEP has more time to influence the dynamics of electrons. Thus a full understanding of CEP's effects on the spectrum for the case of mid-IR driving field is urgently needed.

For this paper, we investigated, both experimentally and theoretically, how CEP's effects on the HHG spectrum differ when driven by mid-IR (1.75 μm) and near-IR (800 nm) laser pulses, respectively. Employing a few-cycle, CEP-stabilized mid-IR driving field, we observed significant CEP effects on the HHG spectrum for different gas media. And by comparing our results to the earlier experimental results for 800 nm obtained by Calegari *et al.*,[23] we found the different features of CEP effects on the HHG spectrum.

*Project supported by the National Natural Science Foundation of China (Grant Nos. 11127901, 61221064, 11134010, 11227902, 11222439, and 11274325), the National Basic Research Program of China (Grant No. 2011CB808103), and the Funds from Shanghai Commission of Science and Technology (Grant No. 12QA1403700).

†Corresponding author. E-mail: yhzheng@mail.siom.ac.cn

‡Corresponding author. E-mail: zhinan_zeng@mail.siom.ac.cn

© 2014 Chinese Physical Society and IOP Publishing Ltd

2. Experiment scheme and results

A schematic diagram of the experimental setup is shown in Fig. 1. The few-cycle ($\sim$ 2 cycles) mid-IR driving laser system (1.75 μm; 1.0 mJ; 12 fs, i.e. 10^{-15} s; CEP stabilized) in our experiment is pumped by a commercial titanium-doped sapphire laser system (40 fs; 800 nm; 1 kHz) and then amplified by a three-stage optical parametric amplifier (OPA). After that an argon-filled hollow fiber (HF) and a pair of fused silica prisms (W) are used to compress the pulse duration and compensate the dispersion respectively. A steel tube with an inner diameter of 1.9 mm and filled with different noble gases (neon, argon, and xenon) is used as the gas cell. To achieve optimal phase match, the gas cell is placed on a high-precision translation stage for movement along the direction of beam propagation. The harmonic signal is produced by using a concave mirror (CM4, focal length is 210 mm) to focus the driving field into the gas cell. Aluminum foil, 150-nm thick, is placed after the gas cell to block the unwanted lower-order harmonics and the residual mid-IR signal. The HHG spectrum is detected by a custom-made spectrometer, made of a spherical concave gold mirror (SCM), a cylindrical concave gold mirror (CCM), a flat-field grating (1200 lines/mm), and a soft-X-ray charge coupled device (CCD). By adjusting the thickness of the prism (W), the CEP of the driving laser pulse can be changed from 0 to 2π.

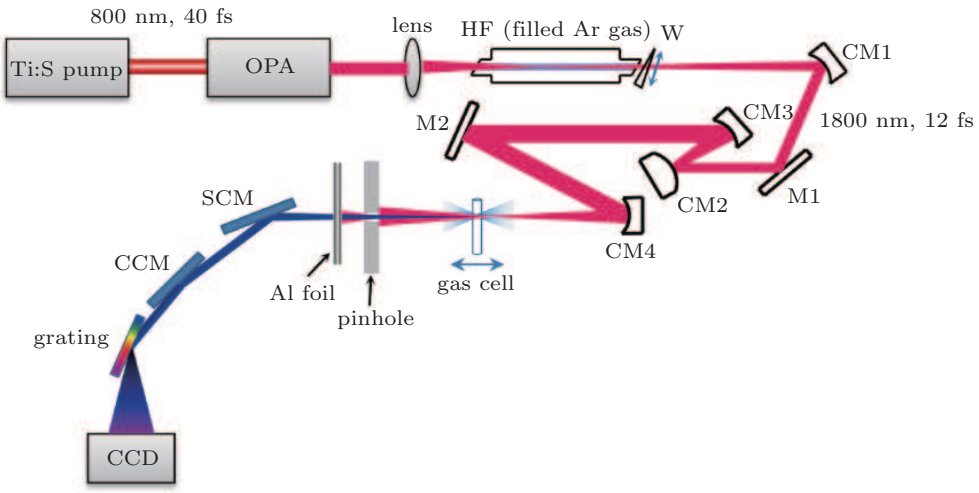


Fig. 1. (color online) Schematic diagram of experimental setup for high-harmonic generation. The CEP is stabilized by a difference frequency generation (DFG) technique in the OPA system. The mid-infrared laser pulse is generated in the OPA and its spectrum is broadened by the argon gas filled hollow fiber (HF). Then the pulse width is compressed by the fused silica prism (W). The convex mirror (CM2) and concave mirror CM3 are used as a beam expander for better phase matching. A harmonic signal is generated by using concave mirror CM4 to focus the driving field into the gas cell. The pinhole and aluminum foil are used to block disturbing signals.

Figure 2(a) shows the original experimental harmonic spectrum detected by CCD as a function of the CEP for neon gas. The CEP is stabilized and changed from -1.5π to 1.5π by tuning the thickness of the fused silica prisms. Three fractions of the signal with relatively high intensity in the spectrum, located around 80 eV, 105 eV, and 145 eV, can be observed. And by changing the CEP, significant periodic variation can be observed in the three intense bands, with a period of π. In addition, the spectral band located around 145 eV varies with CEP with a positive slope. Figure 2(b) shows the original experimental harmonic spectrum for argon gas as a function of CEP. Two separate strong spectra can be seen in Fig. 2(b), located around 80 eV and 105 eV. Similar to the case of neon gas, these two spectral segments vary periodically with CEP with a period of π, but with a much lower contrast. Besides, the intense tilted region of the spectrum around 145 eV is missing for argon gas. Figure 2(c) shows the harmonic spectrum for xenon. Much different from Fig. 2(a) and Fig. 2(b), only one intense spectral region around 75 eV is found, due to the low ionization energy of xenon, and the spectral band varies with CEP periodically, with no obvious slope. Figure 2(d) plots the normalized intensity of harmonic signal at 80 eV as function of the relative CEP for two gas media: neon (blue line) and argon (red line), and figure 2(e) shows the case of the harmonic signal at 105 eV. For neon gas, the CEP varied harmonic signals at photon energy of 80 eV and 105 eV give a better contrast ratio than argon gas; that is, the CEP influences the harmonic spectrum much more for neon gas in those spectral bands, as shown in Fig. 2(d) and Fig. 2(e). This is caused by the excessive ionization of argon gas in the driving field, for the intensity of the driving field ($\sim 2.7 \times 10^{14}$ W/cm^2) has exceeded the saturated intensity ($\sim 2.0 \times 10^{14}$ W/cm^2) for argon gas.

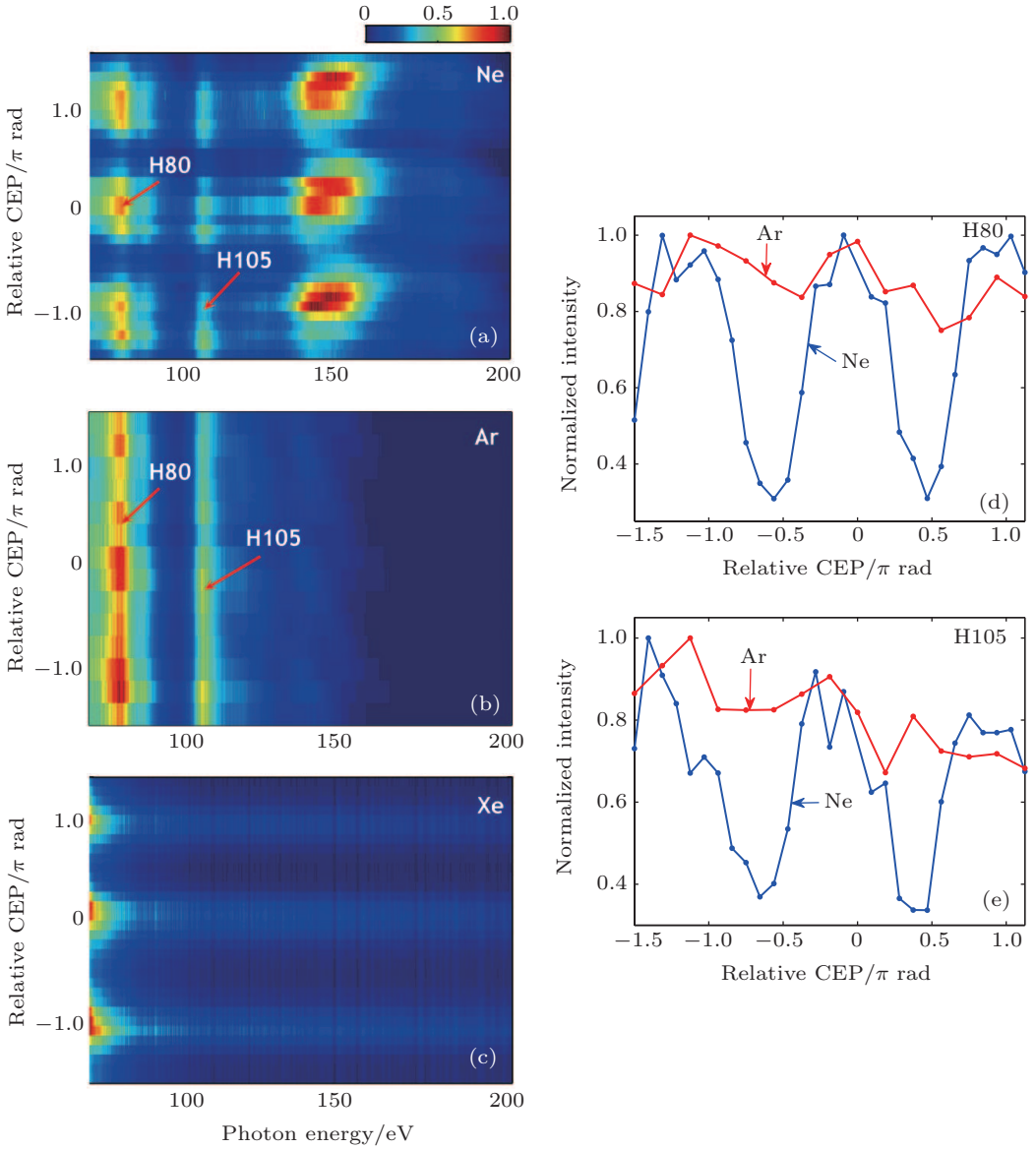


Fig. 2. (color online) Experimental harmonic spectra as functions of the relative CEP for three interaction-gas media: (a) neon, (b) argon, and (c) xenon. (d) Normalized intensity of the selected harmonic signals as a function of CEP at photon energies of 80 eV for neon gas (blue) and argon gas (red); (e) The case of harmonic photon energy at 105 eV. The photon energy in our experiment is calibrated by using the sharp aluminum absorption edge in the spectrum. The central wavelength of the driving field is 1.75 μm, and the full width at half maximum (FWHM) is 12 fs. The CEP is changed from -1.5π to 1.5π.

As we lack CEP-stabilized few-cycle 800-nm laser pulses, we have compared our results with previous work[23] that employed a near-IR laser field with the wavelength of $\sim$ 800 nm. Comparing the results shows that the CEP-varied HHG spectra differ somewhat for mid-IR and near-IR driving fields. These differences can also be seen from the latter part of this paper, since our simulation results for 800-nm laser field are much like the experimental results in Ref. [23]. For further investigation, we performed the following numerical simulation.

3. Numerical simulation

In our simulation, we use the first-order propagation (FOP) equation[24] to calculate the evolution of the laser field and choose the Lewenstein model[8] to get the time-dependent dipole moment of the atom. In addition, in the simulation, the original driving pulse is assumed in Gaussian form both temporally and spatially. We perform the calculations by using both the mid-IR and near-IR driving fields. The wavelength of the mid-IR driving pulse is 1800 nm, the FWHM is 12 fs, the peak intensity is 2.7×10^{14} W/cm^2, and the beam waist is 40 μm. The wavelength of the near-IR driving field is 800 nm; the FWHM is 5.3 fs with the aim of aligning the same optical cycles in one pulse as in the mid-IR case, and the other parameters are the same as in the mid-IR case.

The left and right columns of Fig. 3 show the corresponding simulation results for mid-IR and near-IR driving fields respectively. The simulation results for mid-IR laser pulse reproduce our experiment well, as can be concluded by comparing the left column of Fig. 2 with Fig. 3. The ones for near-IR

driving field are in good agreement with the previous work of Calegari *et al.*,[23] as can be seen by comparing the right column of Fig. 3 with the results in Ref. [23]. As depicted in Fig. 3, by comparing the two kinds of driving fields, for the near-IR case we can see that: the HHG spectrum reaches the cutoff at lower photon energy; the tilted intense fringes have a steeper slope; for different gas media, there are no differences in the trends of the spectra near the cutoff. In the framework of the Lewenstein model, different electron trajectories contribute to the generation of a harmonic signal, the two most relevant being: so-called 'short' trajectories with electron return time close to half an optical period and 'long' trajectories with electron return time close to one optical period. So to show the mechanism more deeply, we analyzed the electron trajectories by time-frequency analysis.[25] A time-frequency spectrogram of the harmonic field $E_{\rm h}(t)$ can be treated as a simultaneous representation of the temporal and spectral characteristics of the harmonic signal. We performed the time-frequency analysis based on the wavelet transform of the harmonic field – the same mechanism chosen by other groups:[23,25]

$$A(t,\omega) = \int E_{\rm h}(t') w_{t,\omega}(t') {\rm d}t', \tag{1}$$

where $w_{t,\omega}(t') = \sqrt{\omega} W[\omega(t'-t)]$ is the wavelet kernel, and the Morlet wavelet[25] is chosen:

$$W(x) = (1/\sqrt{\tau})\, {\rm e}^{{\rm i}x}\, {\rm e}^{-x^2/2\tau^2}. \tag{2}$$

The other groups[23,25] have checked that the absolute value of $A(t,\omega)$ is related to the parameter τ, but the general pattern does not change much. So it is reasonable to keep the parameter τ as a constant throughout the whole calculation. In our work we set $\tau = 15$ to perform the wavelet transform.

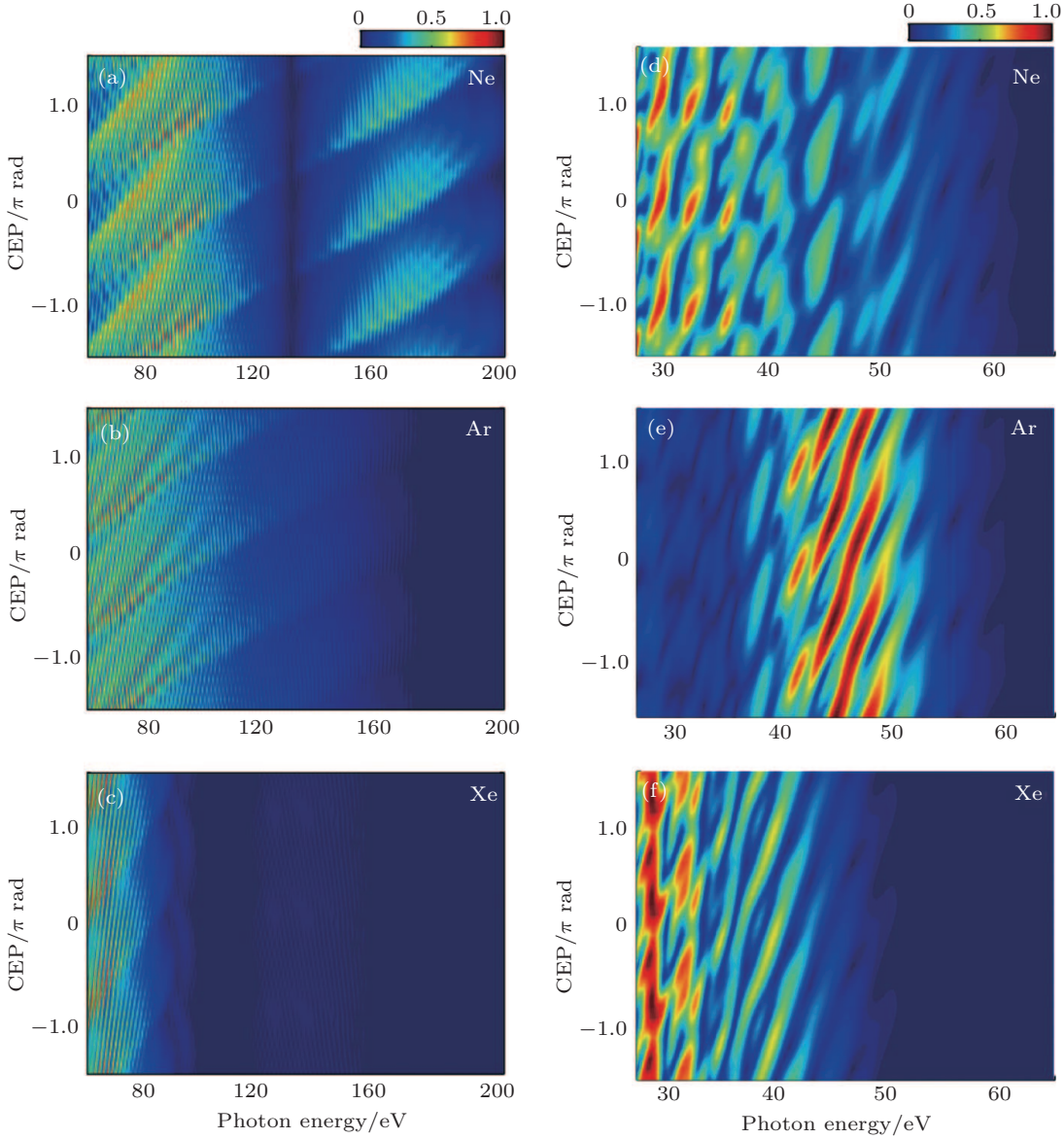


Fig. 3. (color online) Left column shows the simulated HHG spectrum as a function of CEP for three different gas media: (a) neon, (b) argon, and (c) xenon for mid-IR (1800 nm, 12 fs) driving field; the right column shows the simulated HHG spectrum as a function of CEP for three different gas targets, (d) neon, (e) argon, and (f) xenon, for a near-IR (800 nm, 5.3 fs) driving field.

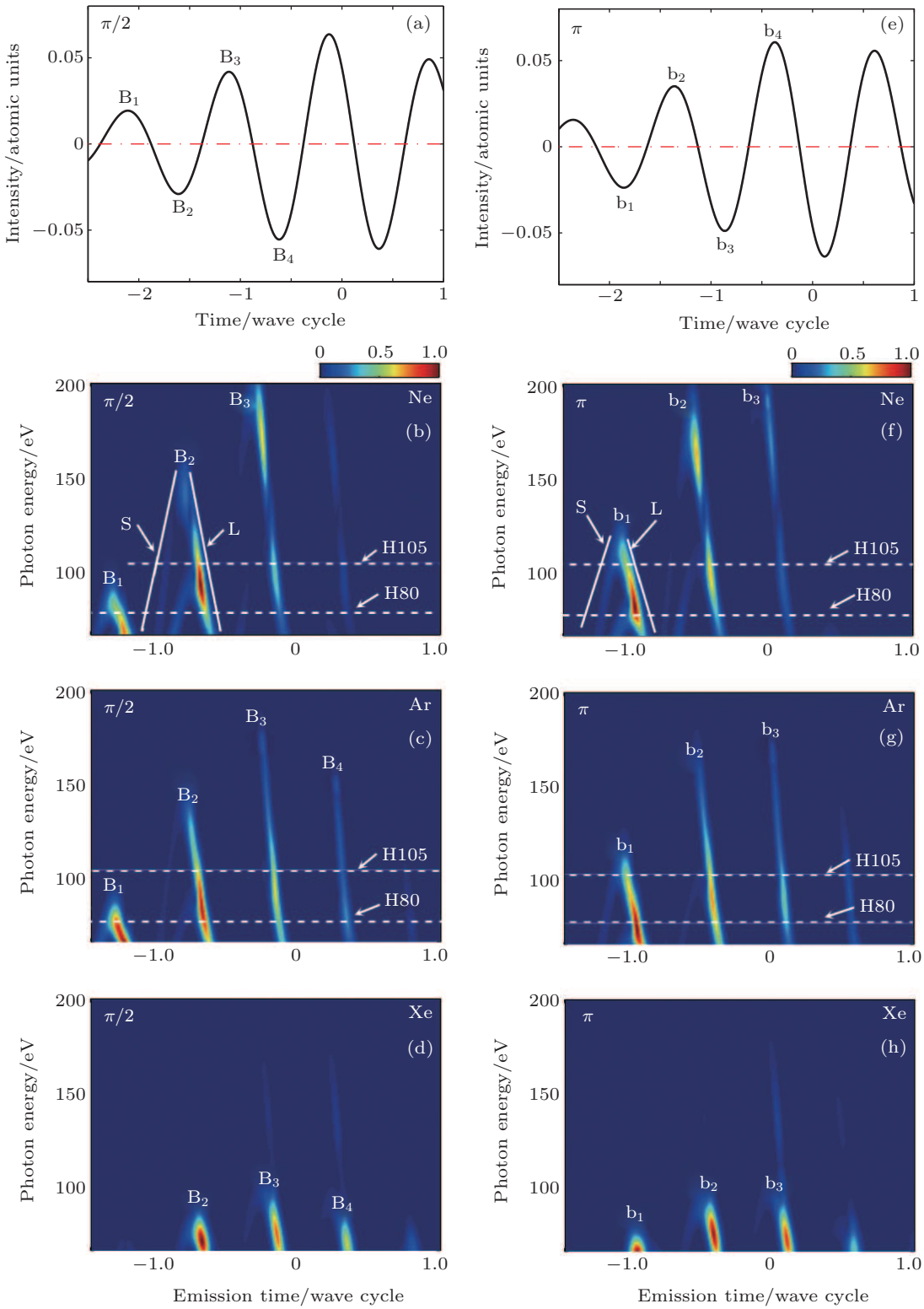


Fig. 4. (color online) The electric field of the driving laser at CEP = $\pi/2$ (a) and π (e). The rest of the sub-figures show time-frequency analysis results for a photon energy range from 70 eV to 200 eV. Panels (b), (c) and (d) show the results at CEP = $\pi/2$ for neon, argon, and xenon gases, respectively. Panels (f), (g) and (h) show the corresponding results at CEP = π for the three gases. The wavelength of the driving field is 1800 nm. For sub-cycle dynamics analysis, we use the label B_i and b_i, with $i = 1, 2, 3, 4, \ldots$, to indicate the approximate half-cycles where the electron is born for CEP = $\pi/2$ and π, respectively. For each B_i (or b_i) electrons can follow 'short' trajectories (S) or 'long' trajectories (L) to recombine with the parent ion, and the white solid line marks the location of each of the trajectories in panels (b) and (f).

Figure 4 shows the evolution of electric field and the time-frequency analysis of the harmonic signal for a driving field with 1800-nm wavelength, and the left and right columns are for CEP = $\pi/2$ and CEP = π, respectively. Figures 4(a) and 4(e) depict the temporal evolution of the driving pulse's electric field. For a given electron trajectory recombination time t_r, the

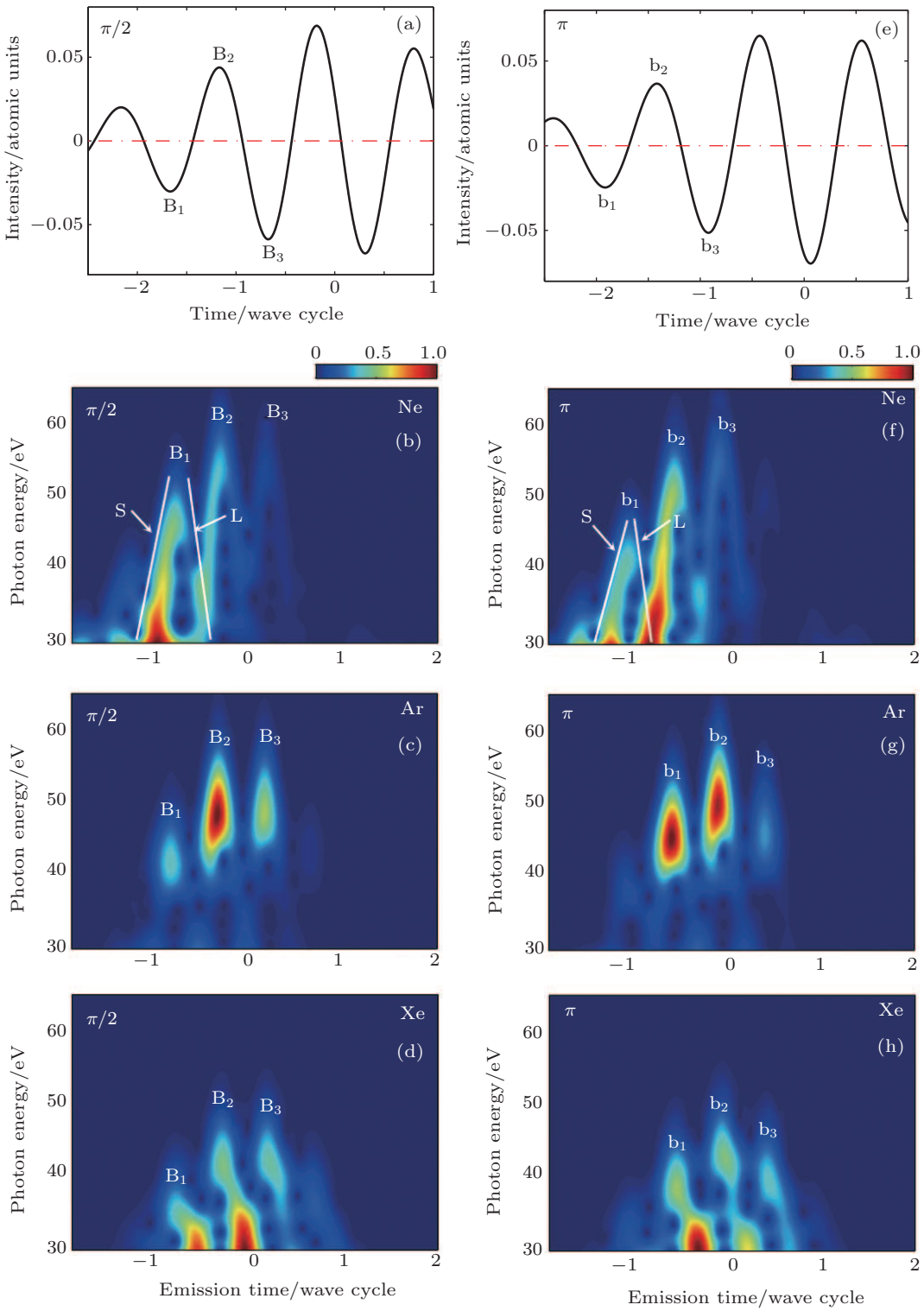


Fig. 5. (color online) The electric field of the driving laser at CEP = $\pi/2$ (a) and π (e). The rest of the sub-figures show time-frequency analysis results for a photon energy range from 28 eV to 65 eV. Panels (b), (c), and (d) show the results at CEP = $\pi/2$ for neon, argon, and xenon gases respectively. Panels (f), (g), and (h) show the corresponding results at CEP = π for the three gases. The wavelength of the driving field is 800 nm. For sub-cycle dynamics analysis, we use the label B_i and b_i, with $i = 1, 2, 3, \ldots$, to indicate the approximate half-cycles where the electron is born for CEP = $\pi/2$ and π, respectively. For each B_i (or b_i) electrons can follow 'short' trajectories (S) or 'long' trajectories (L) to recombine with the parent ion, and the white solid line marks the location of each of the trajectories in panels (b) and (f).

corresponding ionization time t_b (or birth time) can be estimated by solving the following equation[12]

$$0 = x(t_b) - x(t_r) = \int_{t_b}^{t_r} \int_{t_b}^{t} E(t')\mathrm{d}t'\mathrm{d}t, \qquad (3)$$

where $x(t)$ is the path of the electron trajectory, and $E(t)$ is the electric field of the driving laser. As shown in the left (or right) column of Fig. 4, the harmonic signals resulting from electrons born at B_i (or b_i) half-cycle, with $i = 1, 2, 3, \ldots$, are marked

with B_i (or b_i) on the time-frequency spectrogram.[26,27] And judging by the difference of ionization time and recombination time (which can be read from the horizontal axis on the time-frequency spectrogram), one can tell the corresponding electron trajectories' type (say 'short' and 'long' trajectory). In addition, one can approximately judge the electron trajectories' type by the time-frequency spectrogram in another way. As reference [27] states, the 'short' ('long') trajectories in the time-frequency spectrogram have a positive (negative) slope; the symbols 'S' and 'L' in Figs. 4 and 5 are used to indicate the 'short'-trajectory and the 'long'-trajectory harmonics.

Figures 4(b) and 4(f) show the time-frequency analysis results for neon gas; figures 4(c) and 4(g) are for argon gas; figures 4(d) and 4(h) are for xenon gas. For the same gas target, by changing the CEP, the electron trajectories tend to shift horizontally along the time axis, and only the contributions from the 'long' trajectories can be found, as shown in Fig. 4. For neon and argon gas, the positions of two specific harmonics, with photon energy of 80 eV and 105 eV, have been marked by a white dashed line in Fig. 4 and labeled with H80 and H105. One can see that for H80 and H105 only the electron trajectories with the negative slope (corresponding to 'long' trajectories) contribute to the harmonic generation. Figure 5 shows the evolution of electric field and the time-frequency analysis of the harmonic signal for a driving field with wavelength of 800 nm at two CEPs. The same trend of horizontal shift can be seen. However, only the contributions from 'short' trajectories can be found, and the same result can be found in the previous work by Calegari *et al.*[23]

4. Conclusion

In summary, we have investigated, both experimentally and theoretically, the differences in CEP effects on the HHG spectrum driven by mid-IR (1800 nm) and near-IR (800 nm) pulse laser field for different gas media. We kept the same pulse intensity and the same number of optical cycles in one pulse for the two kinds of driving fields. The mid-IR driving field tends to generate the harmonic signal at different photon energy for different CEPs. Moreover, for a different interaction gas medium, the CEP-dependent HHG spectrum of the mid-IR driving field manifests different features, while that of the near-IR driving field does not change much. In addition, the difference in harmonic signals produced by the mid-IR driving field at different CEPs arises mainly from the contribution of 'long' electron trajectories, while for the case of a near-IR-driven laser field, the contributions from 'short' electron trajectories are dominant.

References

[1] Ditmire T, Gumbrell E T, Smith R A, Tisch J W G, Meyerhofer D D and Hutchinson M H R 1996 *Phys. Rev. Lett.* **77** 4756
[2] Bellini M, Lyngå C, Tozzi A, Gaarde M B, Hänsch T W, L'Huillier A and Wahlström C G 1998 *Phys. Rev. Lett.* **81** 297
[3] Chini M, Zhao K and Chang Z 2014 *Nat. Photon.* **8** 178
[4] Corkum P B 1993 *Phys. Rev. Lett.* **71** 1994
[5] Cheng T W, Li X P, Ao S Y and Fu P M 2003 *Chin. Phys. Lett.* **20** 1511
[6] Wang Y S and Xu Z Z 2000 *Chin. Phys. Lett.* **17** 491
[7] Feynman R P and Hibbs A R 1965 *Quantum Mechanics and Path Integrals* (New York: McGraw-Hill Book Company)
[8] Lewenstein M, Balcou P, Ivanov M Y, L'Huillier A and Corkum P B 1994 *Phys. Rev. A* **49** 2117
[9] Lewenstein M, Sali'eres P and L'Huillier A 1995 *Phys. Rev. A* **52** 4747
[10] Lewenstein M, Kulander K C, Schafer K J and Bucksbaum P H 1995 *Phys. Rev. A* **51** 1495
[11] Brabec T and Krausz F 2000 *Rev. Mod. Phys.* **72** 545
[12] Yakovlev V S and Scrinzi A 2003 *Phys. Rev. Lett.* **91** 153901
[13] Zhang J, Zhang J T, Sun Z R and Xu Z Z 2004 *Chin. Phys. Lett.* **21** 468
[14] Wang B B, Chen J, Liu J, Li X P and Fu P M 2005 *Chin. Phys. Lett.* **22** 2237
[15] Baltuska A, Udem T, Uiberacker M, Hentschel M, Goulielmakis E, Gohle C, Holzwarth R, Yakovlev V S, Scrinzi A, Hänsch T W and Krausz F 2003 *Nature* **421** 611
[16] Chipperfield L E, Gaier L N, Knight P L, Marangos J P and Tisch J W G 2005 *J. Mod. Opt.* **52** 243
[17] Haworth C A, Chipperfield L E, Robinson J S, Knight P L, Marangos J P and Tisch J W G 2007 *Nat. Phys.* **3** 52
[18] Sansone G, Benedetti E, Caumes J P, Stagira S, Vozzi C, Nisoli M, Poletto L, Villoresi P, Strelkov V, Sola I, Elouga L B, Zaïr A, Mével E and Constant E 2009 *Phys. Rev. A* **80** 063837
[19] Goulielmakis E, Schultze M, Hofstetter M, Yakovlev V S, Gagnon J, Uiberacker M, Aquila A L, Gullikson E M, Attwood D T, Kienberger R, Krausz F and Kleineberg U 2008 *Science* **320** 1614
[20] Sheehy B, Martin J D D, DiMauro L F, Agostini P, Schafer K J, Gaarde M B and Kulander K C 1999 *Phys. Rev. Lett.* **83** 5270
[21] Liu C, Takashi N, Tetsuo S and Hideaki O 2008 *Phys. Rev. A* **77** 043411
[22] Torres R, Siegel T, Brugnera L, Procino I, Underwood J G, Altucci C, Velotta R, Springate E, Froud C, Turcu I C E, Patchkovskii S, Ivanov M Y, Smirnova O and Marangos J P 2010 *Phys. Rev. A* **81** 051802
[23] Calegari F, Lucchini M, Kim K S, Ferrari F, Vozzi C, Stagira S, Sansone G and Nisoli M 2011 *Phys. Rev. A* **84** 041802
[24] Geissler M, Tempea G, Scrinzi A, Schnürer M, Krausz F and Brabec T 1999 *Phys. Rev. Lett.* **83** 2930
[25] Tong X M and Chu S I 2000 *Phys. Rev. A* **61** 021802
[26] Kamta G L, Bandrauk A D and Corkum P B 2005 *J. Phys. B: At. Mol. Opt. Phys.* **38** L339
[27] Cheng J, Le A T, Trallero-Herrero C A and Lin C D 2011 *Phys. Rev. A* **84** 043411